

Raman-Scattering Measurements and Theory of the Energy-Momentum Spectrum for Underdoped $\text{Bi}_2\text{Sr}_2\text{CaCuO}_{8+\delta}$ Superconductors: Evidence of an s -Wave Structure for the Pseudogap

S. Sakai,^{1,2,3} S. Blanc,⁴ M. Civelli,⁵ Y. Gallais,⁴ M. Cazayous,⁴ M.-A. Méasson,⁴ J. S. Wen,⁶ Z. J. Xu,⁶ G. D. Gu,⁶ G. Sangiovanni,^{7,8} Y. Motome,² K. Held,⁸ A. Sacuto,⁴ A. Georges,^{1,3,9,10} and M. Imada^{2,3}

¹Centre de Physique Théorique, École Polytechnique, CNRS, 91128 Palaiseau, France

²Department of Applied Physics, University of Tokyo, Hongo, Tokyo 113-8656, Japan

³JST-CREST, Hongo, Bunkyo-ku, Tokyo 113-8656, Japan

⁴Laboratoire Matériaux et Phénomènes Quantiques (UMR 7162 CNRS), Université Paris Diderot-Paris 7, Bâtiment Condorcet, 75205 Paris Cedex 13, France

⁵Laboratoire de Physique des Solides, Université Paris-Sud, CNRS, UMR 8502, F-91405 Orsay Cedex, France

⁶Matter Physics and Materials Science, Brookhaven National Laboratory (BNL), Upton, New York 11973, USA

⁷Institut für Theoretische Physik und Astrophysik, Universität Würzburg, Am Hubland, D-97074 Würzburg, Germany

⁸Institute for Solid State Physics, Vienna University of Technology, 1040 Vienna, Austria

⁹Collège de France, 11 Place Marcelin Berthelot, 75005 Paris, France

¹⁰DPMC, Université de Genève, 24 Quai Ernest Ansermet, CH-1211 Genève, Suisse

(Received 28 January 2013; published 3 September 2013)

We reveal the full energy-momentum structure of the pseudogap of underdoped high- T_c cuprate superconductors. Our combined theoretical and experimental analysis explains the spectral-weight suppression observed in the B_{2g} Raman response at finite energies in terms of a pseudogap appearing in the single-electron excitation spectra above the Fermi level in the nodal direction of momentum space. This result suggests an s -wave pseudogap (which never closes in the energy-momentum space), distinct from the d -wave superconducting gap. Recent tunneling and photoemission experiments on underdoped cuprates also find a natural explanation within the s -wave pseudogap scenario.

DOI: [10.1103/PhysRevLett.111.107001](https://doi.org/10.1103/PhysRevLett.111.107001)

PACS numbers: 74.72.Kf, 71.10.Fd, 79.60.-i

The superconducting gap of high- T_c cuprate superconductors has a d -wave symmetry [1] with zero-point nodes in momentum space, in contrast to the nodeless s -wave gap of conventional superconductors. In the underdoped regime, another gap, called a pseudogap, exists even above the critical temperature T_c . The relation between pseudo- and superconducting gaps has been a controversial issue whose understanding may provide long-sought insights into the mechanism of high-temperature superconductivity [2–9]. According to a broad class of theories, the pseudogap is a continuation of the superconducting gap into a regime of incoherent Cooper pairs. A competing class of theories holds instead that the pseudogap is a manifestation of a new instability; therefore, it should be different from the superconducting gap. Most of these theories [10–15] assume a d -wave structure of pseudogap, since angle-resolved photoemission spectroscopy (ARPES) [16] has observed the pseudogap vanishing in the nodal region in a fashion reminiscent of a d -wave superconducting gap. Nevertheless, ARPES can only access the occupied side of the electronic spectra. Therefore, the determination of the complete structure of the pseudogap is an essential ingredient missing in order to unveil the real connection between the pseudo- and superconducting gaps.

In this Letter, we explore the pseudogap structure on the “dark” (unoccupied) side of underdoped cuprates, by combining cellular dynamical mean-field theory (CDMFT) [17]

with Raman-spectroscopy experiments. In stark contrast with the assumption of a d -wave pseudogap, we find an s -wave pseudogap which accounts for various anomalous properties of the nodal (B_{2g}) and antinodal (B_{1g}) Raman responses, as well as of ARPES and scanning tunneling microscopy (STM). Our study focuses on the pseudogap phase above T_c , leaving open the question about possible competing orders under the superconducting dome, where quantum oscillation experiments on $\text{YBa}_2\text{Cu}_3\text{O}_{6.5}$ [18,19] have revealed a dramatic reconstruction of the electronic structure.

Raman B_{2g} (B_{1g}) spectroscopy, obtained from cross polarizations along (45° from) the Cu-O bonds [20], has been performed on an underdoped $\text{Bi}_2\text{Sr}_2\text{CaCuO}_{8+\delta}$ ($\text{Bi}2212$) single crystal, grown with a floating zone method ($T_c = 74$ K). The hole-doping concentration $p \sim 0.11$ has been achieved by changing the oxygen content only. A triple grating spectrometer (JY-T64000) equipped with a nitrogen cooled CCD detector was used. All the measurements have been corrected for the Bose factor and the instrumental spectral response and are thus proportional to the imaginary part of the Raman response function.

For the theoretical analysis, we have adopted a minimal model of the Cu-O planes: The two-dimensional Hubbard model with the (next-)nearest-neighbor transfer integral $t(t' = -0.2t)$ and the on-site Coulomb repulsion $U = 8t$. CDMFT has been implemented on a 16-site cluster [21], which is much larger than the four-site cluster previously

used [22–30], and is solved with the continuous-time quantum Monte Carlo method [31] [except for the case of Fig. 2(f), where the exact diagonalization method for a 2×2 cluster was employed]. The momentum-dependent quantities have been extracted from the cluster by using the cumulant interpolation scheme [27] (see Refs. [21,30]).

In order to avoid a severe sign problem in the continuous-time quantum Monte Carlo method, we are forced to adopt a theoretical doping $p_{\text{th}} = 0.05$ smaller than the experimental $p \sim 0.11$. However, our goal is to identify general doping-independent properties of the pseudogap phase rather than to simulate a specific material at a specific doping. We shall therefore trace a qualitative comparison between theory and experiments, and in order to facilitate it, we (i) provide an order-of-magnitude value by setting the energy scale of our theory $t = 0.3$ eV [32] (1 eV $\sim 1.2 \times 10^4$ K $\sim 8.1 \times 10^3$ cm $^{-1}$) and (ii) divide by a factor of 1.5 the theoretical energy scales directly related to the pseudogap amplitude because the pseudogap energy scale at 5% doping is about 1.5 times larger than that at 11% [16,33].

Figure 1(a) presents the theoretical spectral weight $A(\mathbf{k}, \omega)$ plotted along the $(\pi, 0)$ – $(\pi/2, \pi/2)$ \mathbf{k} cut [labeled “a” in Fig. 1(b)]. Here, we focus on the low-energy region shaded on the local density of states (DOS) in Fig. 1(c). We find a coherent dispersing quasiparticle band (black circles) crossing the Fermi level ($\omega = 0$) in the nodal region $\mathbf{k} \sim (\pi/2, \pi/2)$, and a less dispersive and less coherent band (white squares) at positive energies $\sim 0.5t$. We call this latter an in-gap band because it arises inside the Mott gap [the wide $0 < \omega < 4t$ region in Fig. 1(c)]. Between these two bands, a gap opens, which we identify with the pseudogap observed in cuprates. The most striking feature is that our pseudogap never vanishes in the energy-momentum space, even in the nodal direction. Hence, differently from the d -wave superconducting gap, it has an s -wave symmetry [23,24] with no node. This structure nevertheless looks like a d wave if observed in the negative-energy plane because the nodal region is gapless below the Fermi level. Several numerical calculations [22–24,34] on smaller clusters without any *a priori* assumption have also indicated a similar pseudogap structure. In our theory, the pseudogap is a pure outcome of the parent Mott insulator [10]. The appearance of a strong-scattering surface in the energy-momentum space [dotted blue line in Fig. 1(a)] drives the metallic system into the Mott insulator by suppressing spectral weight [15,23,25–27,35,36]. As this surface is closer to the Fermi level in the antinodal than in the nodal region [23], a (pseudo)gap in the spectra opens around $\omega = 0$ at the antinodes while it shifts to positive energies in the nodal region [22,23,27], where a Fermi arc is observed [Fig. 1(b)].

Experimentally, there are few studies on the momentum structure of the unoccupied spectra. ARPES at a relatively high temperature can detect spectra slightly above the Fermi level by analyzing thermally populated states. For an underdoped Bi2212 sample ($T_c = 65$ K, $p \sim 0.09$) at $T = 140$ K, Yang *et al.* [6] obtained the unoccupied spectra below

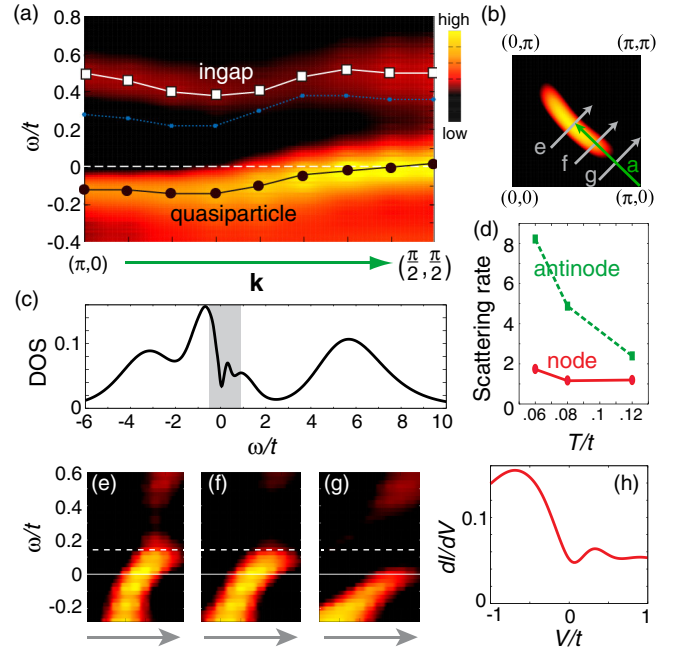


FIG. 1 (color online). Theoretical spectral intensity at $T = 0.06t$ and $p_{\text{th}} = 0.05$ (a) in the energy-momentum space and (b) in the first quadrant of the Brillouin zone at low energy ($\omega \sim 0$). Black circles and white squares denote, respectively, the peak positions of quasiparticle and in-gap bands, which are separated by an s -wave pseudogap. The dotted blue curve plots the position of the maximal-scattering rate (i.e., the imaginary part of self-energy) at each momentum. The green (dark gray) arrow in (b) denotes the momentum cut used in (a). (c) Local DOS in a wide energy range displaying the Hubbard bands ($\omega < 0$ and $\omega \sim 6t$). The shaded area denotes the low-energy region plotted in (a). (d) Temperature dependence of the scattering rate within the pseudogap at $\omega = 0.36t$ (node) and $0.28t$ (antinode). (e)–(g) Spectral function along the cuts depicted in (b), comparable to available ARPES data [6]. The dashed line indicates the upper energy limit reached in Figs. 3(e)–3(g) of Ref. [6]. (h) Tunneling conductance at $T = 0.06t$, comparable to, e.g., Fig. 5(b) (inset) of Ref. [38].

0.04 eV. These results [reproduced in Figs. S1(e)–S1(g) in the Supplemental Material [39]] are in good agreement with our theoretical spectra; see Figs. 1(e)–1(g). A dashed white line in each panel indicates the positive-energy window, which we estimate was accessed in the ARPES experiment. In the nodal direction [Fig. 1(e)], the pseudogap opens above the window and the electronic dispersion close to the Fermi level appears rather symmetric. In moving to the antinodal region [Fig. 1(g)], the pseudogap shifts down into the energy window and the electronic dispersion displays a marked electron-hole asymmetry. This again evidences a radical difference between pseudogap and superconducting gap, whose hallmark is represented by two particle-hole-symmetric Bogoliubov bands.

The tunneling conductance dI/dV , albeit missing momentum resolution, can also provide valuable information on the unoccupied spectra. In Fig. 1(h), we plot the theoretical tunneling conductance calculated by $dI/dV = -\int d\omega f'(\omega - eV)D(\omega)$, where f' is the energy derivative

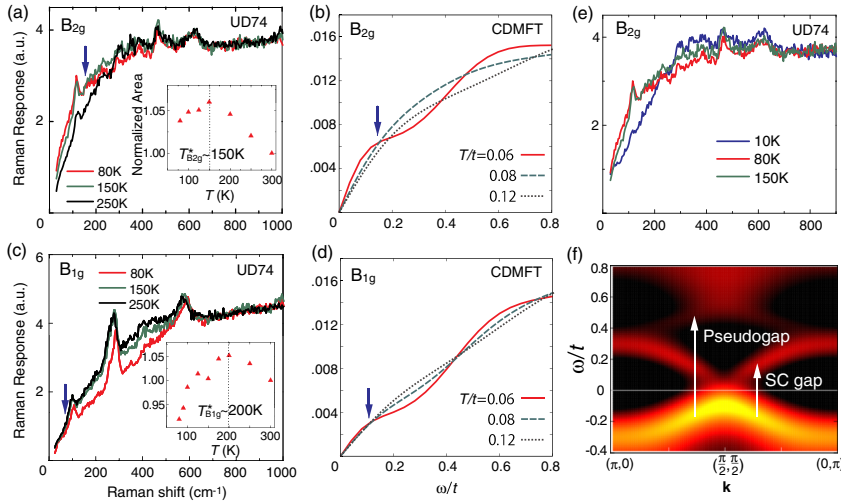


FIG. 2 (color online). B_{2g} Raman spectra obtained by experiments (a) on an underdoped Bi2212 ($T_c \sim 74$ K, $p \sim 0.11$) and by the CDMFT (b) in the underdoped regime ($p_{th} = 0.05$). (c), (d) The same for B_{1g} spectra. The blue arrows mark the starting energy points of pseudogap depression. The insets in (a) and (c) plot the integrated Raman weight normalized at $T = 300$ K as a function of temperature. (e) Experimental B_{2g} Raman response in the normal ($T = 150$ and 80 K) and superconducting ($T = 10$ K) states. In (a), (c), and (e), the red (light gray), green (gray), black, and blue (dark gray) curves correspond respectively to 80 K, 150 K, 250 K, and 10 K. (f) Theoretical spectral intensity calculated with CDMFT+exact diagonalization method for a 2×2 cluster in the superconducting state. The white arrows denote excitations beyond the pseudo- and superconducting (SC) gaps in the nodal region, which contribute to the B_{2g} Raman intensity.

of the Fermi distribution function f , $-e$ is the electron charge, and $D(\omega)$ is the cluster density of states. First of all, the dI/dV curve has a smaller weight on the unoccupied side, reflecting the underlying projective nature of strong correlation [37]. The hump around $V = 0.4t$ reflects the in-gap band at positive energies seen in Fig. 1(a). The s -wave pseudogap predominantly opening on the unoccupied side elucidates a further asymmetric shape in the dI/dV curve, which is observed by STM for strongly underdoped samples [see, e.g., the inset in Fig. 5(b) of Ref. [38]]. For a more quantitative comparison with ARPES and STM results, see Secs. II and IV in the Supplemental Material [39].

However, ARPES [6] and STM [38] are limited, respectively, in energy range and in momentum resolution. Hence, key information about the presence of a gap in the *unoccupied* spectra in the *nodal* region is still missing in experiments. We have therefore performed Raman spectroscopy [33], which, albeit in a less direct way, can separately access the nodal (B_{2g}) and antinodal (B_{1g}) electronic structures, as well as the wide energy region above the Fermi level.

Theoretical Raman spectra have been calculated within the bubble approximation from the CDMFT single-particle spectra

$$\chi''_{\mu}(\omega) = 2 \int \frac{d\mathbf{k}}{(2\pi)^2} \gamma_{\mu}^2(\mathbf{k}) \int_{-\infty}^{\infty} d\omega' A(\mathbf{k}, \omega') A(\mathbf{k}, \omega + \omega') \times [f(\omega') - f(\omega + \omega')] \quad (1)$$

with $\gamma_{B_{1g}} = 1/2[\cos(k_x) - \cos(k_y)]$ and $\gamma_{B_{2g}} = \sin(k_x) \times \sin(k_y)$. This is known to give a reasonable estimate for a B_{2g} response [40], on which our main result of s -wave pseudogap relies. Vertex corrections can be more significant in B_{1g} geometry. However, a recent study [41] based on the dynamical cluster approximation [42] shows that the corrections are still small in a low-energy region where the antinodal pseudogap opens. These considerations together with the nice correspondence with the experimental results (as we will show in the following) support our theoretical analysis.

We first point out that the CDMFT Raman spectra [Figs. 2(b) and 2(d)] well reproduce the rather broad incoherent electronic response observed in experiments [Figs. 2(a) and 2(c)]. This broad feature is the outcome of mixing low-energy coherent quasiparticle excitations with incoherent high-energy ones (e.g., the Hubbard bands), which are captured within CDMFT. This description would not be possible by approaches employing only low-energy quasiparticles.

Second, in the B_{2g} (nodal) response, the slope at $\omega = 0$, which is proportional to the quasiparticle lifetime, increases with lowering temperature, both in experiments [Fig. 2(a)] and in theory [Fig. 2(b)] [43]. This behavior is consistent with a metallic Fermi arc observed around the node by ARPES [16] and within CDMFT [Fig. 1(b)] [21–24,26–28,44]. The low-energy slope of the B_{1g} (antinodal) response shows instead little temperature dependence [Figs. 2(c) and 2(d)] [33,45–47]. This signals a nonmetallic behavior at the antinodes, where the pseudogap indeed opens at the Fermi level [22–24,27,28,44,48,49].

We now look at the behavior of the B_{2g} [B_{1g}] response in the intermediate-energy interval ($0.15t$ – $0.45t$ [$0.1t$ – $0.45t$] in CDMFT and 150 – 600 [50 – 600] cm^{-1} in experiments), whose onset is indicated by the blue arrow in Figs. 2(a)–2(d). In this energy range, a depression should result from the appearance of a pseudogap. The nontrivial fact is that this depression takes place not only in the B_{1g} symmetry, where one expects to see the antinodal pseudogap, but also in the B_{2g} symmetry. The interval of the depression in the B_{2g} [B_{1g}] theoretical Raman response is $0.3t \sim 480 \text{ cm}^{-1}$ [$0.35t \sim 560 \text{ cm}^{-1}$] wide (taking into account the above-mentioned factor 1.5 due to the difference between p and p_{th}), in a good agreement with the experimental value 450 [550] cm^{-1} . Notice that the energy endpoint of the B_{2g} depression is nearly equal to that of B_{1g} : 600 cm^{-1} in experiment and $0.45t$ in theory. A similar depression in the B_{2g} response was previously reported for other underdoped cuprates [46,47,50], where

it was attributed to the gap opening at the Fermi level away from the node. However, our study reveals a novel mechanism due to a gap above the Fermi level in the nodal region, as we shall explain below.

Another remarkable property is that the antinodal ($T_{B_{1g}}^*$) and nodal ($T_{B_{2g}}^*$) pseudogap-crossover temperatures are different. In the insets of Figs. 2(a) and 2(c), we plot the area under the electronic response (up to 800 cm^{-1}) as a function of temperature. The maxima provide an estimation of the pseudogap-crossover temperature $T_{B_{2g}}^* \sim 150 \text{ K}$ and $T_{B_{1g}}^* \sim 200 \text{ K}$. In the CDMFT result for the intermediate energies, while the B_{1g} response monotonically decreases from $T = 0.12t$ to $0.06t$ [Fig. 2(d)], the B_{2g} response is not monotonic: It increases from $T = 0.12t$ to $0.08t$ and then decreases by further lowering the temperature to $T = 0.06t$ [Fig. 2(b)]. Thus, we find two different crossover temperatures in the CDMFT results, too: $T_{B_{2g}}^* \sim 0.08t \sim 180 \text{ K}$ and $T_{B_{1g}}^* \geq 0.12t \sim 280 \text{ K}$ (again taking into account the factor 1.5), still in reasonable agreement with the experimental values. We summarize these comparisons of energy scales in Sec. I of the Supplemental Material [39].

We now analyze the Raman response in terms of the CDMFT spectra $A(\mathbf{k}, \omega)$. In Fig. 3(a), sandwiched in between the quasiparticle peak (black bullets) close to the Fermi level and an in-gap peak (white squares) at $\omega \sim 0.5t$, a depression (arrow) smoothly continues from the antinode to the node. This has been identified with the pseudogap in Fig. 1(a). This pseudogap depression in $A(\mathbf{k}, \omega)$ originates the depression in the Raman responses [see Eq. (1)], as indeed seen in Figs. 2(b) and 2(d). In particular, the presence of the pseudogap at positive energy in the nodal region leads to the depression in the B_{2g} Raman response in the intermediate-energy interval. In Fig. 3(b), the pseudogap persists up to $T = 0.12t$ around the antinode, while it is almost lost at $T = 0.08t$ around the node, consistently with the difference between $T_{B_{2g}}^*$ and $T_{B_{1g}}^*$ observed in the Raman spectra. The difference originates from different temperature dependences of scattering rates in the nodal and antinodal regions, as extensively reported in experiments [16,33,46] and as shown in Fig. 1(d), where the CDMFT nodal and antinodal maximal-scattering rates within the pseudogap are plotted against temperature.

We finally turn to the experimental Raman response in the superconducting state and show that it also supports the s -wave pseudogap. Figure 2(e) compares the B_{2g} responses below and above T_c . In general, upon the opening of a superconducting gap below T_c , spectral weight is removed from the Fermi level. This is true also for a d -wave superconducting gap around the nodal point. Accordingly, the B_{2g} Raman response decreases at low energy ($\omega < 200 \text{ cm}^{-1}$) and increases at higher energy ($200 \text{ cm}^{-1} < \omega < 700 \text{ cm}^{-1}$). Interestingly, the latter increase emerges mostly within the pseudogap energy range ($150 \text{ cm}^{-1} < \omega < 600 \text{ cm}^{-1}$). A similar behavior was reported also in $\text{YBa}_2\text{Cu}_3\text{O}_{7-x}$, $\text{Bi}_2\text{Sr}_2(\text{Ca}_{0.62}\text{Y}_{0.38})\text{Cu}_2\text{O}_{8+\delta}$ [46,50], and $\text{HgBa}_2\text{CuO}_{4+\delta}$

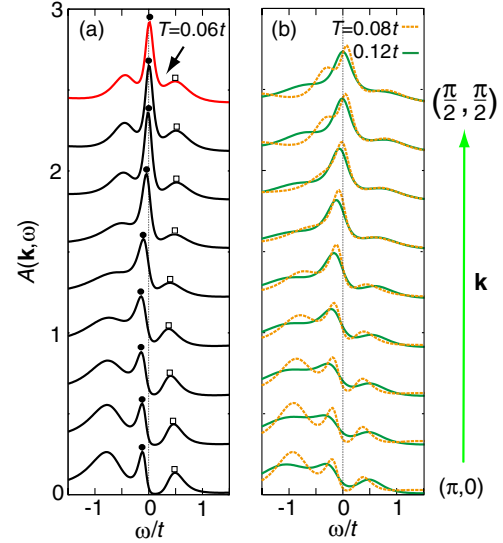


FIG. 3 (color online). Energy distribution curves of the single-particle spectra along the $(\pi, 0) - (\pi/2, \pi/2)$ line (a) at $T = 0.06t$ and (b) at $T = 0.08t$ and $0.12t$. The black circles (white squares) denote the quasiparticle (in-gap) peak plotted in Fig. 1(a). The arrow at the top curve denotes the pseudogap. For clarity, the curves are offset by 0.3.

[47], showing that it is common to various cuprates. This suggests that the superconducting gap is substantially smaller than the pseudogap, particularly in the nodal region. Namely, the Bogoliubov quasiparticle bands emerge below T_c in the nodal region inside the pseudogap energy range. This scenario is illustrated in the explanatory Fig. 2(f), which plots a 2×2 CDMFT $A(\mathbf{k}, \omega)$ in the superconducting state [30] along the momentum-space cut $(\pi, 0) - (\pi/2, \pi/2) - (0, \pi)$. Here, we use a simple $\cos k_x - \cos k_y$ form (which is widely supported in experiments [16]) for interpolating the CDMFT d -wave superconducting gap. In particular, around the node, the superconducting gap is smaller than the pseudogap, as depicted by the white arrows. This competition between pseudo- and superconducting gaps is consistent with other cluster DMFT studies [29,51,52].

In conclusion, by combining Raman experiment and CDMFT, we have explored the unoccupied part of the single-particle spectra of an underdoped cuprate and found that the pseudogap opens *above* the Fermi level in the nodal region. The pseudogap thus shows a strongly electron-hole-asymmetric s -wave structure, distinct from the d -wave superconducting gap. This suggests that they have different origins. To obtain this result, it has been crucial to shed light on the empty part (dark side) of the electronic spectrum. This region should therefore be the focus of future experimental (e.g., along the lines of Refs. [5–9]) and theoretical (as focused in Refs. [24,36]) developments.

We acknowledge valuable comments by A. Tremblay. M. Ci. acknowledges discussions with V. Brouet, A. Cano, B. G. Kotliar, I. Paul, and A. Santander-Syro. The work was supported by a Grant-in-Aid for Scientific Research (Grant No. 22340090) from MEXT, Japan. A part of

the research has been funded by the Strategic Programs for Innovative Research (SPIRE), MEXT, and the Computational Materials Science Initiative (CMSI), Japan. K. H. is supported by the Austrian Science Fund (FWF) through SFB ViCoM F4103-N13, and G. S. by the FWF under “Lise-Meitner” Grant No. M1136. S. B., Y. G., M. Ca., M.-A.M., and A. S. acknowledge support from l’Agence Nationale de la Recherche through Grant No. BLAN07-1-183876, “GAPSUPRA.” The work in BNL is supported by the DOE under Contract No. DE-AC02-98CH10886. The calculations were performed at the Vienna Scientific Cluster and at the Supercomputer Center, ISSP, University of Tokyo.

-
- [1] C. C. Tsuei, J. R. Kirtley, Z. F. Ren, J. H. Wang, H. Raffy, and Z. Z. Li, *Nature (London)* **387**, 481 (1997).
- [2] M. R. Norman, D. Pines, and C. Kallin, *Adv. Phys.* **54**, 715 (2005).
- [3] S. Hüfner, M. A. Hossain, A. Damascelli, and G. A. Sawatzky, *Rep. Prog. Phys.* **71**, 062501 (2008); M. Le Tacon, A. Sacuto, A. Georges, G. Kotliar, Y. Gallais, D. Colson, and A. Forget, *Nat. Phys.* **2**, 537 (2006).
- [4] A. J. Millis, *Science* **314**, 1888 (2006).
- [5] A. Kanigel, U. Chatterjee, M. Randeria, M. Norman, G. Koren, K. Kadowaki, and J. Campuzano, *Phys. Rev. Lett.* **101**, 137002 (2008).
- [6] H.-B. Yang, J. D. Rameau, P. D. Johnson, T. Valla, A. Tsvelik, and G. D. Gu, *Nature (London)* **456**, 77 (2008).
- [7] M. Hashimoto *et al.*, *Nat. Phys.* **6**, 414 (2010).
- [8] R.-H. He *et al.*, *Science* **331**, 1579 (2011).
- [9] J. E. Hoffman, *Nat. Phys.* **6**, 404 (2010).
- [10] P. W. Anderson, *Science* **235**, 1196 (1987).
- [11] V. J. Emery and S. A. Kivelson, *Nature (London)* **374**, 434 (1995).
- [12] S. Chakravarty, R. B. Laughlin, D. K. Morr, and C. Nayak, *Phys. Rev. B* **63**, 094503 (2001).
- [13] L. Balents, M. P. A. Fisher, and C. Nayak, *Int. J. Mod. Phys. B* **12**, 1033 (1998).
- [14] M. Franz and Z. Tesanovic, *Phys. Rev. Lett.* **87**, 257003 (2001).
- [15] K.-Y. Yang, T. M. Rice, and F.-C. Zhang, *Phys. Rev. B* **73**, 174501 (2006).
- [16] A. Damascelli, Z. Hussain, and Z.-X. Shen, *Rev. Mod. Phys.* **75**, 473 (2003).
- [17] G. Kotliar, S. Y. Savrasov, G. Palsson, and G. Biroli, *Phys. Rev. Lett.* **87**, 186401 (2001).
- [18] N. Doiron-Leyraud, C. Proust, D. LeBoeuf, J. Levallois, J.-B. Bonnemaïson, R. Liang, D. A. Bonn, W. N. Hardy, and L. Taillefer, *Nature (London)* **447**, 565 (2007).
- [19] S. E. Sebastian, N. Harrison, E. Palm, T. P. Murphy, C. H. Mielke, R. Liang, D. A. Bonn, W. N. Hardy, and G. G. Lonzarich, *Nature (London)* **454**, 200 (2008).
- [20] T. P. Devereaux, D. Einzel, B. Stadlober, R. Hackl, D. Leach, and J. Neumeier, *Phys. Rev. Lett.* **72**, 396 (1994).
- [21] S. Sakai, G. Sangiovanni, M. Civelli, Y. Motome, K. Held, and M. Imada, *Phys. Rev. B* **85**, 035102 (2012).
- [22] B. Kyung, S. S. Kancharla, D. Sénéchal, and A.-M. S. Tremblay, *Phys. Rev. B* **73**, 165114 (2006).
- [23] S. Sakai, Y. Motome, and M. Imada, *Phys. Rev. Lett.* **102**, 056404 (2009).
- [24] S. Sakai, Y. Motome, and M. Imada, *Phys. Rev. B* **82**, 134505 (2010).
- [25] D. Sénéchal and A.-M. S. Tremblay, *Phys. Rev. Lett.* **92**, 126401 (2004).
- [26] M. Civelli, M. Capone, S. S. Kancharla, O. Parcollet, and G. Kotliar, *Phys. Rev. Lett.* **95**, 106402 (2005).
- [27] T. D. Stanescu and G. Kotliar, *Phys. Rev. B* **74**, 125110 (2006).
- [28] A. Liebsch and N.-H. Tong, *Phys. Rev. B* **80**, 165126 (2009).
- [29] M. Civelli, M. Capone, A. Georges, K. Haule, O. Parcollet, T. Stanescu, and G. Kotliar, *Phys. Rev. Lett.* **100**, 046402 (2008).
- [30] M. Civelli, *Phys. Rev. B* **79**, 195113 (2009).
- [31] E. Gull, A. J. Millis, A. I. Lichtenstein, A. N. Rubtsov, M. Troyer, and P. Werner, *Rev. Mod. Phys.* **83**, 349 (2011).
- [32] O. K. Andersen, A. I. Lichtenstein, O. Jepsen, and F. Paulsen, *J. Phys. Chem. Solids* **56**, 1573 (1995).
- [33] T. P. Devereaux and R. Hackl, *Rev. Mod. Phys.* **79**, 175 (2007).
- [34] T. Tohyama, *Phys. Rev. B* **70**, 174517 (2004).
- [35] C. Berthod, T. Giamarchi, S. Biermann, and A. Georges, *Phys. Rev. Lett.* **97**, 136401 (2006).
- [36] Y. Yamaji and M. Imada, *Phys. Rev. Lett.* **106**, 016404 (2011).
- [37] P. W. Anderson and N. P. Ong, *J. Phys. Chem. Solids* **67**, 1 (2006); P. W. Anderson, *Nat. Phys.* **2**, 626 (2006).
- [38] A. Pushp, C. V. Parker, A. N. Pasupathy, K. K. Gomes, S. Ono, J. Wen, Z. Xu, G. Gu, and A. Yazdani, *Science* **324**, 1689 (2009).
- [39] See Supplemental Material <http://link.aps.org/supplemental/10.1103/PhysRevLett.111.107001> for a detailed comparison (including that of energy scales) with various experimental results and for a discussion on the relation to the theoretical results obtained by relevant methods.
- [40] T. P. Devereaux and A. P. Kampf, *Phys. Rev. B* **59**, 6411 (1999).
- [41] N. Lin, E. Gull, and A. J. Millis, *Phys. Rev. Lett.* **109**, 106401 (2012).
- [42] T. Maier, M. Jarrell, T. Pruschke, and M. H. Hettler, *Rev. Mod. Phys.* **77**, 1027 (2005).
- [43] Note that sharp peaks (e.g., at $\sim 120\text{ cm}^{-1}$ in B_{2g} and at $\sim 280\text{ cm}^{-1}$ in B_{1g}) in Figs. 2(a) and 2(c) stem from phonon excitations, which we will not consider in our study.
- [44] A. Macridin, M. Jarrell, T. Maier, P. R. C. Kent, and E. D’Azevedo, *Phys. Rev. Lett.* **97**, 036401 (2006).
- [45] F. Venturini, M. Opel, T. Devereaux, J. Freericks, I. Tüttő, B. Revaz, E. Walker, H. Berger, L. Forró, and R. Hackl, *Phys. Rev. Lett.* **89**, 107003 (2002).
- [46] M. Opel *et al.*, *Phys. Rev. B* **61**, 9752 (2000).
- [47] Y. Gallais, A. Sacuto, T. P. Devereaux, and D. Colson, *Phys. Rev. B* **71**, 012506 (2005).
- [48] M. Ferrero, P. Cornaglia, L. De Leo, O. Parcollet, G. Kotliar, and A. Georges, *Phys. Rev. B* **80**, 064501 (2009).
- [49] N. Lin, E. Gull, and A. J. Millis, *Phys. Rev. B* **82**, 045104 (2010).
- [50] R. Nemetshchek, M. Opel, C. Hoffmann, P. Müller, R. Hackl, H. Berger, L. Forró, A. Erb, and E. Walker, *Phys. Rev. Lett.* **78**, 4837 (1997).
- [51] G. Sordi, P. Sémon, K. Haule, and A.-M. S. Tremblay, *Phys. Rev. Lett.* **108**, 216401 (2012).
- [52] E. Gull, O. Parcollet, and A. J. Millis, *Phys. Rev. Lett.* **110**, 216405 (2013).